

A Trio of Metal-Rich Dust and Gas Disks Found Orbiting Candidate White Dwarfs with K -Band Excess

J. Farihi^{1*}, B. T. Gänsicke², P. R. Steele³, J. Girven², M. R. Burleigh¹,
E. Breedt² and D. Koester⁴

¹*Department of Physics Astronomy, University of Leicester, Leicester LE1 7RH, UK*

²*Department of Physics, University of Warwick, Coventry CV4 7AL, UK*

³*Max Planck Institut für Astrophysik, D-85741 Garching, Germany*

⁴*Institut für Theoretische Physik und Astrophysik, University of Kiel, 24098 Kiel, Germany*

ABSTRACT

This paper reports follow-up photometric and spectroscopic observations, including warm *Spitzer* IRAC photometry of seven white dwarfs from the SDSS with apparent excess flux in UKIDSS K -band observations. Six of the science targets were selected from 16 785 DA star candidates identified either spectroscopically or photometrically within SDSS DR7, spatially cross-correlated with HK detections in UKIDSS DR8. Thus the selection criteria are completely independent of stellar mass, effective temperature above 8000 K, and the presence (or absence) of atmospheric metals. The infrared fluxes of one target are compatible with a spatially-unresolved late M or early L-type companion, while three stars exhibit excess emissions consistent with warm circumstellar dust. These latter targets have spectral energy distributions similar to known dusty white dwarfs with high fractional infrared luminosities (thus the K -band excesses). Optical spectroscopy reveals the stars with disk-like excesses are polluted with heavy elements, denoting the ongoing accretion of circumstellar material. One of the disks exhibits a gaseous component – the fourth reported to date – and orbits a relatively cool star, indicating the gas is produced via collisions as opposed to sublimation, supporting the picture of a recent event. The resulting statistics yield a lower limit of 0.8% for the fraction dust disks at DA-type white dwarfs with cooling ages less than 1 Gyr. Two overall results are noteworthy: all stars whose excess infrared emission is consistent with dust are metal-rich; and no stars warmer than 25 000 K are found to have this type of excess, despite sufficient sensitivity.

Key words: circumstellar matter— planetary systems— stars: abundances— stars: low mass stars— brown dwarfs— stars: evolution— white dwarfs

1 INTRODUCTION

Near-infrared photometry of white dwarfs examines a scientific phase space that is difficult or impossible to probe for main-sequence stars. The first to recognize this potential was Probst (1981), who realized the compact nature of white dwarfs allowed a straightforward photometric detection of very cool stellar and substellar companions. Brown dwarfs, which often require sophisticated detection techniques when searched for at main-sequence stars, are up to 10 times larger than a typical white dwarf and can be readily detected in *spatially-unresolved* observations as excess near-infrared flux (Probst 1983). Thus, white dwarfs are an excellent tool for

studies of the low-mass stellar and substellar mass function via companions (Farihi et al. 2005; Zuckerman & Becklin 1992; Probst & O’Connell 1982). Photometry with *Spitzer* has extended this potential to include closely orbiting brown dwarfs and massive planets although no candidates are yet apparent (Farihi et al. 2008b; Mullally et al. 2007).

Another way in which near-infrared photometry of white dwarfs is advantageous is that circumstellar dust orbiting within the Roche limit of the stellar remnant becomes heated sufficiently to emit in this wavelength range (Kilic et al. 2006). This potential is precluded for main-sequence stars because the analogous spatial region, where km-size or larger solid bodies are tidally destroyed, does not extend significantly above their surfaces (Davidsson 1999). Furthermore, any material generated in that narrow region

* E-mail: jf123@star.le.ac.uk

Table 1. Multi-Wavelength Photometry and Derived Parameters for SDSS White Dwarfs

SDSS Prefix	0959	1159 ^a	1221	1247	1320	1506	1557
Spectral Type	DAZ	DQp	DAZ	DA	DA	DA	DAZ
Spectroscopic Data	WHT	SDSS	WHT	SDSS	SDSS	WHT	SDSS+WHT
α (J2000; h m s)	09 59 04.69	11 59 33.10	12 21 50.81	12 47 40.93	13 20 44.68	15 06 26.18	15 57 20.77
δ (J2000; $^{\circ}$ ' ")	-02 00 47.6	+13 00 31.6	+12 45 13.3	+10 35 56.1	+00 18 54.9	+06 38 45.9	+09 16 24.6
FUV (0.15 μ m; AB mag)	...	> 20	19.55 \pm 0.06	18.23 \pm 0.02	16.52 \pm 0.03	18.40 \pm 0.02	18.03 \pm 0.02
NUV (0.23 μ m; AB mag)	...	19.62 \pm 0.09	18.78 \pm 0.02	18.33 \pm 0.01	16.76 \pm 0.01	17.31 \pm 0.01	18.16 \pm 0.01
<i>u</i> (0.36 μ m; AB mag)	18.52 \pm 0.02	18.22 \pm 0.03	18.54 \pm 0.02	18.63 \pm 0.02	17.08 \pm 0.02	16.96 \pm 0.01	18.50 \pm 0.02
<i>g</i> (0.47 μ m; AB mag)	18.09 \pm 0.03	18.14 \pm 0.02	18.19 \pm 0.02	18.50 \pm 0.01	17.13 \pm 0.01	16.57 \pm 0.01	18.45 \pm 0.01
<i>r</i> (0.62 μ m; AB mag)	18.36 \pm 0.02	17.75 \pm 0.01	18.40 \pm 0.02	18.82 \pm 0.02	17.47 \pm 0.02	16.63 \pm 0.01	18.81 \pm 0.01
<i>i</i> (0.75 μ m; AB mag)	18.54 \pm 0.02	17.70 \pm 0.02	18.56 \pm 0.02	19.13 \pm 0.02	17.72 \pm 0.02	16.79 \pm 0.01	19.13 \pm 0.01
<i>z</i> (0.89 μ m; AB mag)	18.88 \pm 0.06	17.82 \pm 0.02	18.86 \pm 0.05	19.33 \pm 0.06	18.05 \pm 0.03	16.93 \pm 0.01	19.34 \pm 0.04
<i>J</i> (1.25 μ m; mag)	18.32 \pm 0.06	17.40 \pm 0.03	18.43 \pm 0.07	18.95 \pm 0.08	17.62 \pm 0.04	16.41 \pm 0.01	18.82 \pm 0.06
<i>H</i> (1.64 μ m; mag)	18.17 \pm 0.09	17.32 \pm 0.06	18.39 \pm 0.10	18.90 \pm 0.11	17.71 \pm 0.08	16.37 \pm 0.02	19.03 \pm 0.14
<i>K</i> (2.20 μ m; mag)	17.62 \pm 0.11	17.08 \pm 0.08	18.01 \pm 0.15	18.47 \pm 0.20	17.53 \pm 0.11	16.35 \pm 0.03	18.35 \pm 0.15
IRAC1 (3.55 μ m; μ Jy)	80 \pm 4	42 \pm 2	40 \pm 5	25 \pm 2	35 \pm 2	75 \pm 4	35 \pm 2
IRAC2 (4.49 μ m; μ Jy)	76 \pm 4	28 \pm 2	40 \pm 6	17 \pm 2	25 \pm 2	50 \pm 3	40 \pm 2
T_{eff} (K)	13280 \pm 20	9500 \pm 500	12250 \pm 20	18540 \pm 150	20220 \pm 180	10670 \pm 10	22810 \pm 40
$\log g$ (cm s^{-2})	8.06 \pm 0.03	8.0	8.20 \pm 0.03	7.86 \pm 0.03	8.37 \pm 0.04	8.21 \pm 0.03	7.54 \pm 0.01
M (M_{\odot})	0.64 \pm 0.02	0.59	0.73 \pm 0.02	0.54 \pm 0.02	0.86 \pm 0.02	0.73 \pm 0.02	0.42 \pm 0.01
d (pc)	203 \pm 4	110 \pm 00	180 \pm 4	396 \pm 9	150 \pm 4	71 \pm 2	566 \pm 2
IR Excess ^b	Dust	Atm	Dust	dM/L	Bkgd	None	Dust

Note. Ultraviolet, optical, and near-infrared photometry are from *GALEX* (Martin et al. 2005), SDSS (Abazajian et al. 2009), and UKIDSS (Lawrence et al. 2007) respectively. For stars with multiple spectroscopic or photometric datasets, table values are the weighted average of available measurements. The SDSS photometry is given in PSF magnitudes; the only catalog entries appropriate for point sources. Stellar parameters are derived by fitting the Balmer line profiles as described in §3.

^aThis star was selected independently from the six primary science targets (see §3.2).

^bSee §3 for the various infrared excess descriptions.

above the star will rapidly dissipate due to radiation pressure and drag forces. Thus, while asteroids and comets commonly pass sufficiently close to the Sun, and presumably other main-sequence stars that host planetary systems, the tidal disruption and subsequent accretion of this debris can only be witnessed at white dwarfs (and possibly neutron stars; Wang et al. 2006).

This paper reports warm *Spitzer* IRAC measurements and optical spectroscopy of six white dwarf candidates selected for apparent *K*-band excess fluxes based on the ground-based photometric surveys the Sloan Digital Sky Survey (SDSS) and the UKIRT Infrared Deep Sky Survey (UKIDSS). Target selection criteria and survey data are given in §2, along with a description of the *Spitzer* and ground-based observations. The spectroscopic and photometric data analysis is presented in §3, with a summary of the overall results in §4.

2 TARGET SELECTION AND OBSERVATIONS

The six primary science targets were selected as described in detail by Girven et al. (2011). Briefly summarizing, DA white dwarf candidates were selected both photometrically and spectroscopically from within SDSS DR7 (Abazajian et al. 2009), and spatially cross-correlated with sources in the UKIDSS (Lawrence et al. 2007) DR4 (and later DR8). A *ugriz* color selection was implemented based on the Eisenstein et al. (2006) SDSS DR4 white dwarf catalog, which was then used to select and download spectra

for 7444, and photometry (only) for 9341, DA star candidates with $g < 19$ AB mag. Cross-correlation with UKIDSS DR8 then resulted in 1884 objects in common with both *H*- and *K*-band detections; these were all fitted with white dwarf atmospheric models to probe for *K*-band photometric excess. Of these 1884 cross-correlated sources, 147 objects were identified as having an infrared excess, including 12 objects (7 spectroscopic and 5 photometric only) in which the excess was most pronounced in the *K*-band, and compatible with either a brown dwarf later than L7 or a dust disk; the UKIDSS data alone could not typically distinguish between those two possibilities.

Six disk candidate white dwarfs found in this manner were selected as targets for *Spitzer* Cycle 6 observations, and are listed in Table 1. Two of these targets (1320 and 1557) were independently identified by Steele et al. (2011). They performed a cross-correlation of the white dwarf catalogs of Eisenstein et al. (2006) and McCook & Sion (1999) with UKIDSS DR8 to identify stars with excess emission via optical and infrared colors, as well as spectral fitting. A seventh target, the DQ peculiar white dwarf LP 494-12 (SDSS 1159; Eisenstein et al. 2006) was selected on the basis of an independent measurement of *K*-band excess (Farihi 2009), corroborated by its UKIDSS photometry.

2.1 Optical Spectroscopy

Of the six primary science targets, SDSS spectra were available within SDSS DR7 for 1247, 1320, and 1557. In addition, long slit spectroscopy was obtained for 0959, 1221, 1506, and

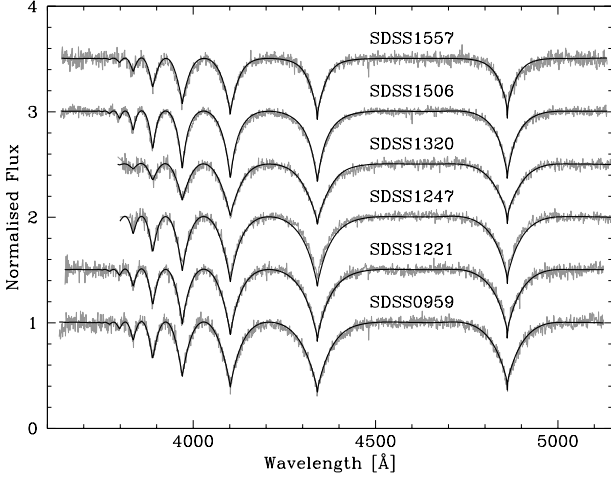


Figure 1. Normalized SDSS and WHT spectra of the six DA white dwarfs in the study are shown in gray, along with the best fit models plotted in black. The SDSS spectra stop at 3800 Å. The WHT spectra of 0959, 1221, and 1557 each contain a narrow absorption line near 4481 Å, that is due to Mg II.

1557 during two observing runs in 2010 April and May using using ISIS, the dual beam spectrograph mounted on the 4.2 m William Herschel Telescope (WHT). The primary aim of these observations was to corroborate the photometrically selected DA candidates (0959, 1221, 1506) and to improve on the SDSS spectroscopy of 1557. For this purpose, the R600 grating was used in the blue arm with a 1'' slit and a 2 (spectral) by 3 (spatial) pixel binning. This setup covered the wavelength range 3650 – 5120 Å, i.e., the entire Balmer series except H α , with an average dispersion of 0.88 Å per binned pixel in the blue arm, and 7691 – 9184 Å with 0.99 Å per binned pixel in the red arm. The red spectra had relatively low signal-to-noise ratio (S/N).

The blue spectra were de-biased and flat-fielded using the STARLINK¹ packages KAPPA and FIGARO and then optimally extracted using the PAMELA² code (Marsh 1989). The extracted spectra were wavelength calibrated using CuNe and CuAr arc lamp exposures, and finally flux calibrated using observations of appropriate standard stars obtained with the same instrumental setup. The photometric classification of 1221, 1506, and 1557 as hydrogen dominated white dwarfs was confirmed by the ISIS spectroscopy. Normalized WHT and SDSS spectra of all *Spitzer* DA targets are shown in Figure 1.

Additional observations of 0959 and 1320 were obtained with the VLT using X-Shooter (D’Odorico et al. 2006) in service mode in 2010 June–July and 2011 February–March. The raw frames were reduced using the X-Shooter pipeline version 1.3.7 within GASGANO³. The standard recipes were used with default settings to extract and wavelength calibrate each spectrum. The final extraction of the science and spectrophotometric standard spectra was carried out using

Table 2. Independent *JHK* Photometry

Star	<i>J</i> (mag)	<i>H</i> (mag)	<i>K_s</i> (mag)
1221 ^a	18.49 ± 0.05	18.21 ± 0.05	18.05 ± 0.05
1221 ^b	18.50 ± 0.05	18.27 ± 0.05	18.22 ± 0.10
1320 ^a	17.64 ± 0.05	17.44 ± 0.05	17.49 ± 0.05
1320 ^b	17.60 ± 0.05	17.61 ± 0.07	17.58 ± 0.11
1557	19.05 ± 0.05	18.92 ± 0.05	18.56 ± 0.05

^aAperture photometry

^bPSF-fitting photometry

APALL within IRAF. Finally, the instrumental response was removed by dividing each observation by the response function, calculated by dividing the associated standard by its corresponding flux table.

2.2 Additional Near-Infrared Photometry

Independent near-infrared photometry for 1221, 1320, and 1557 was obtained on the 23 March 2011 with the WHT using the Long-Slit Intermediate Resolution Infrared Spectrograph (LIRIS; Machado et al. 1998). Images taken in a 9-point dither pattern were obtained in the *J*-, *H*-, and *K_s*-band filters (MKO system; R. Karjalainen 2011, private communication) with typical total exposure times of 270 s in clear conditions. Three standard star (ARNICA; Hunt et al. 1998) fields were observed in a similar manner for photometric zero-point calibration. The data were reduced in the standard manner, by subtracting a median sky from each image in the dithered stack, flat-fielding (using sky flats), then averaging and recombining frames.

LIRIS suffers from what is known as a detector reset anomaly, which appears in certain frames as a discontinuous jump (in dark current) between the upper and the lower two quadrants. To remove this unwanted signal, after flat-fielding and sky subtraction, the detector rows were collapsed into a median column (with real sources rejected), and subsequently subtracted from the entire two dimensional image. The resulting fully reduced frames exhibit smooth backgrounds, free of the anomalous gradient.

Aperture photometry of standard stars was performed using $r = 3''.75$ aperture radii and sky annuli of $5'' - 7''.5$ in size. For the relatively faint science targets, smaller photometric apertures were employed with corrections derived from several brighter stars within the same image field and filter. For both 1221 and 1320, point-spread function (PSF) fitting (i.e., DAOPHOT) was used in addition to photometry with small apertures. All data taken in the *K_s*-band filter were flux-calibrated using the ARNICA *K*-band standard star photometry, and the error introduced by this should be significantly smaller than the 5% absolute calibration uncertainty. The independent *JHK_s* photometry is listed in Table 2.

¹ Developed and maintained by the Joint Astronomy Centre and available from <http://starlink.jach.hawaii.edu/starlink>

² Developed and maintained by T. R. Marsh and available from <http://www.warwick.ac.uk/go/trmarsh>

³ <http://www.eso.org/sci/software/gasgano>

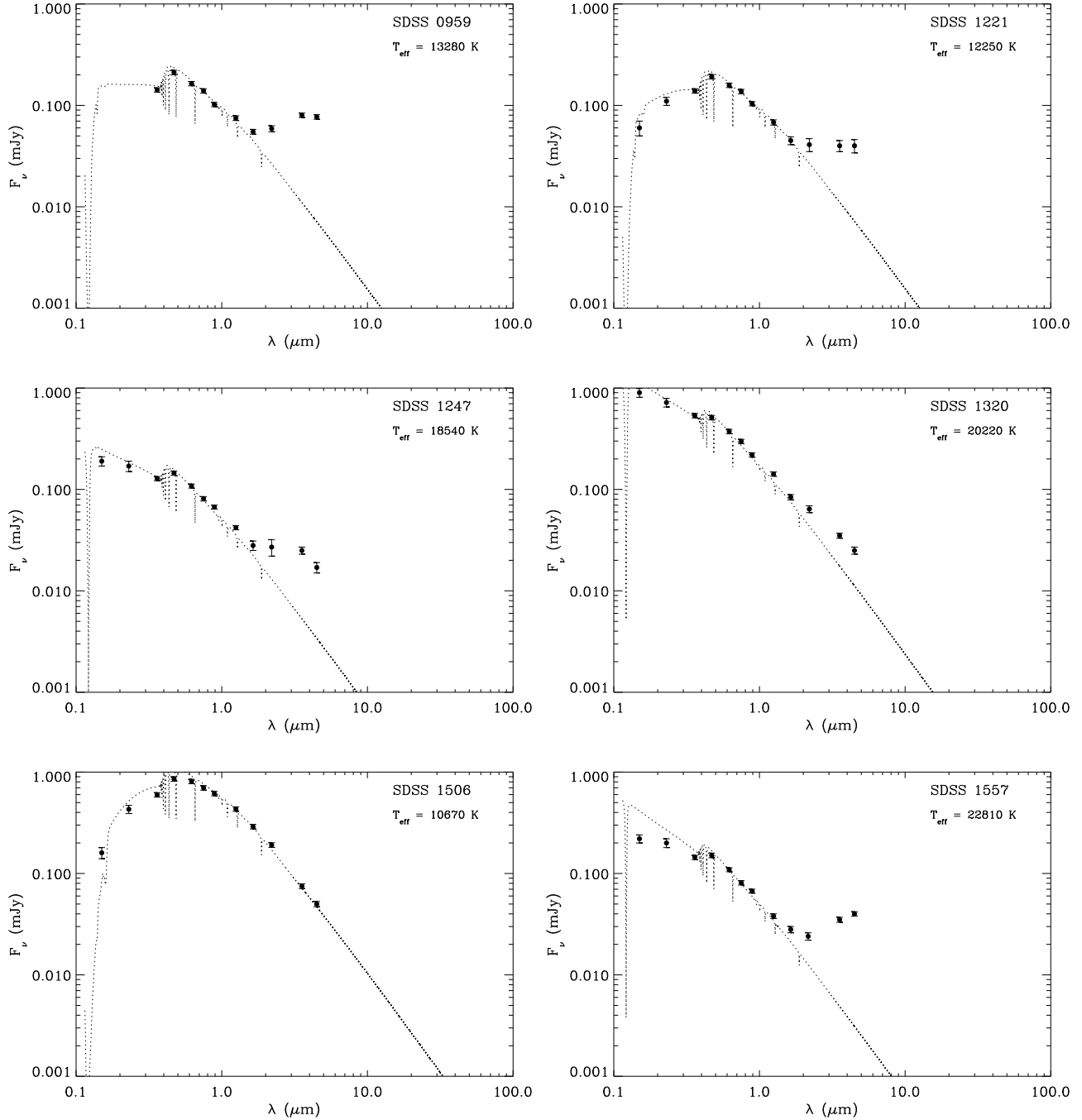


Figure 2. Ultraviolet through infrared spectral energy distributions of the DA-type, infrared excess candidates. Stellar atmosphere models are plotted as dotted lines, using parameters derived from model fits to hydrogen Balmer lines in the SDSS or WHT spectra, and matched to the observed *g*-band fluxes. Table 1 photometry is shown as data points with error bars.

2.3 *Spitzer* IRAC Observations

Near-infrared imaging observations of the white dwarf targets were obtained with the warm *Spitzer Space Telescope* (Werner et al. 2004) during Cycle 6 using the Infrared Array Camera (IRAC; Fazio et al. 2004) at 3.6 and 4.5 μm . The total integration time in each channel was 1200 s, where the observations consisted of 40 frames taken in the cycling (medium) dither pattern with 30 s individual exposures. All

images were analyzed and fluxes measured as in Farihi et al. (2010b) using 0.6 pixel^{-1} mosaics created using MOPEX. In cases where the flux of a neighboring source was a potential contaminant of the white dwarf photometry (i.e., 1221 and 1247, see §3.1), steps were taken to minimize or remove any such external contributions, including small aperture photometry and PSF fitting with DAOPHOT and APEX.

Of all IRAC targets, only 1506 is detected in the *WISE* Preliminary Data Release. Reliable data exists only

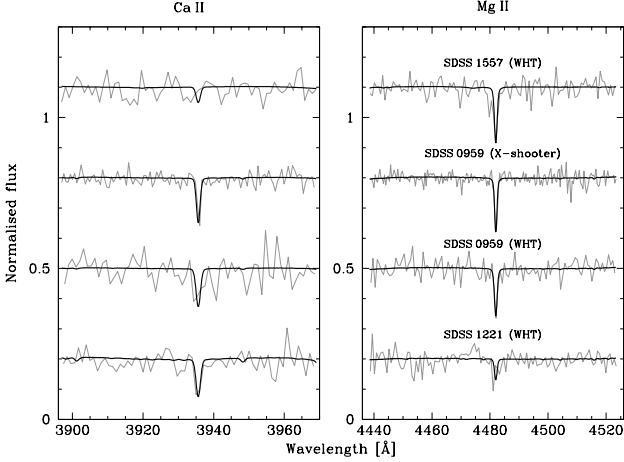


Figure 3. Black lines are model fits to the Ca II 3934 Å and Mg II 4481 Å line regions in the normalized ISIS and X-Shooter spectra, plotted in gray, of all three white dwarfs found to have circumstellar dust. The stars are displayed top-to-bottom by decreasing effective temperature: 22 810 K, 13 280 K, 12 250 K.

at $3.4 \mu\text{m}$, where the flux ($76 \pm 8 \mu\text{Jy}$) is in agreement with the IRAC photometry, albeit with larger errors. Generally, the science targets are too faint for *WISE*, where confusion can be a serious concern (see Melis et al. 2011), and hence the choice of warm *Spitzer*.

3 RESULTS AND ANALYSIS

The SDSS and WHT spectra of the six DA white dwarfs were fitted using model atmosphere spectra computed with the code described by Koester (2010), and following the method described by Rebassa-Mansergas (2007). In brief, the grid of model spectra was fitted to the normalized Balmer line profiles, leading to a ‘hot’ and ‘cold’ solution of roughly equal absorption line equivalent width. This degeneracy is broken by fitting the models also to the slope of the flux-calibrated spectra. The best-fit models are overplotted on the data in Figures 1 and 2, and the parameters are reported in Table 1.

All targets stars but one reveal excess emission at IRAC wavelengths when compared to the atmospheric models, derived from their optical spectroscopy. However, there are only four genuine cases where the excess radiation is associated with an additional component physically associated with the system: three dust disks and one (likely) low-mass stellar companion. All individual stars are discussed below in some detail.

3.1 New Disk-Polluted White Dwarfs

Three stars – 0959, 1221, 1557 – display infrared fluxes consistent with dust disks orbiting within their respective Roche limits for large asteroids. The excess emissions are too strong, and the infrared colors are incorrect for substellar or planetary companions (Farihi et al. 2009, 2008a). Specifically, even for the case of a substellar object with anomalously red colors, the 4.5μ flux requires its size to be

Table 3. Relative Number Abundances in Disk-Polluted Stars

Object	$\log (\text{Mg}/\text{H})$	$\log (\text{Ca}/\text{H})$	Mg/Ca
Sun	−4.45	−5.66	16
Chondrites	−0.72	−1.96	17
0959	−5.2	−7.0	59
1221	< −5.6	−7.5	< 85
1557	−4.5	< −5.7	> 15

Note. Measured abundance uncertainties are 0.2 dex.

several to ten times that of Jupiter, in contrast with observations and models of brown dwarfs and planets Leggett et al. (2010). Firmly corroborating the disk interpretation, each of these DA white dwarfs was found to be metal-lined in follow up WHT and VLT optical spectroscopy, consistent with ongoing infall of circumstellar material. Specifically, their ISIS spectra contain narrow absorption lines near 3934 Å and 4481 Å, which are due to Ca II K and Mg II, respectively; they are DAZ stars. Figure 3 displays model fits to the detected metal absorption features, using TLUSTY and SYNPEC (Hubeny & Lanz 1995; Lanz & Hubeny 1995) in order to estimate the photospheric abundances.

Only Mg and Ca are detected, and Table 3 reports the determined abundances and upper limits for these two elements. The Mg/Ca ratio observed in 0959 is significantly larger than that found in chondrites, but similar to that found for the highly polluted white dwarf GALEX 1931 (Vennes et al. 2011), where the relative poverty of Ca, Ti, and Al is potentially consistent with the removal of crust and mantle in a differentiated, terrestrial-like body during the post-main sequence evolution of the star (Melis et al. 2011). The Mg abundances determined from the X-Shooter and ISIS spectra of 0959 are consistent to within the errors, while the low S/N around the Ca II K line prevents a meaningful abundance estimate for that element based on the ISIS data. For 1221 and 1557, only upper limits are derived for Mg and Ca respectively, partly due to the inferior quality of the ISIS spectra compared to the X-Shooter data. However, another factor is that the undetected atomic transitions are not easily excited at the respective effective temperature of these stars (Zuckerman et al. 2003).

For all three stars, the excess infrared emissions are fitted with optically thick, flat disk models (Jura 2003). As discussed in previous white dwarf-disk studies, optically thin dust models are inferior, primarily due to the Poynting-Robertson timescales involved (von Hippel et al. 2007). Not only would such dust be removed on the timescale of years, but the particles orbit once every few hours, ensuring the disk will relax rapidly into a flat configuration; a geometrically thin, optically thick disk circumvents these issues. Importantly, such a disk can harbor sufficient dust mass to account for the most highly polluted helium atmosphere stars (Farihi et al. 2010a), whereas an optically thin disk cannot (Jura et al. 2009).

The fitted disk parameters are listed in Table 4, and the model fluxes are shown together with the observational data in Figure 4. For each star, R/d is derived from the atmospheric models using the spectroscopically derived stellar parameters and observed photometry: R is determined from T_{eff} and $\log g$ while d is specified by $m - M$ for the same

Table 4. Disk Parameters

Star	T_{eff} (K)	R/d (10^{-12})	T_{in} (K)	T_{out}^a (K)	r_{in} (R_*)	r_{out}^a (R_*)	$\cos i$
0959	13280	1.37	1600	800	10	25	1.0
1221	12250	1.41	1400	800	11	23	0.7
1557	22810	0.73	1400	800	25	52	0.5

^aOwing to the wavelength coverage, the outer disk temperature and radius is not as well-constrained by the data as the inner disk temperature. See §3.1 for a detailed discussion of uncertainties in the disk parameters.

(e.g., $g - M_g$, $r - M_r$). For fixed R/d , there are three free parameters for a flat disk; inner disk edge temperature, outer disk edge temperature, and inclination. These models contain a modest amount of degeneracy in their ability to fit the data, even when longer wavelength data, such as 8 and $24 \mu\text{m}$ photometry are available (Jura et al. 2007). However, the models provide good, if broad constraints on the geometry and temperature of the disks. The inner disk edge is fairly well constrained by the excess emission at 2.2 and $3.6 \mu\text{m}$, but not uniquely so, while the $4.5 \mu\text{m}$ flux can be reproduced by a relatively wide temperature range and a higher inclination, or a narrower temperature range and a lower inclination. This is because the total disk emission is a function of its temperature profile and solid angle, and the latter is comprised of the inclination and the ring annuli.

Despite this uncertainty, the infrared excesses cannot be satisfactorily fit with inner disk temperatures below 1200 K, nor with significant amounts of $T < 500$ K dust. These new discoveries essentially mimic the thermal emission profiles observed at 16 dusty white dwarfs with longer wavelength data in addition to the wavelengths covered by warm *Spitzer* (Farihi et al. 2010b). The excess at 0959 is sufficiently strong that it requires a nearly face-on disk, while the disk inclinations for 1221 and 1557 are less constrained. Importantly, the excesses are consistent with inner disk temperatures approaching or exceeding that which causes rapid sublimation of typical dust grains; gas thus produced gives rise to viscous drag and enhances inflow of disk material onto the stellar surface (Rafikov 2011). While the outer disk temperatures are not more tightly bound, the range of acceptable values places all the debris within $1.5 R_\odot$, where large, solid bodies will be shredded. Overall, the data are consistent with circumstellar debris originating in large, star-grazing solid bodies that is now being gradually falling onto the stellar surface.

3.1.1 0959

This white dwarf displays Ca II emission lines that are the hallmark of closely-orbiting metallic gas. These emission features are clearly detected in the X-shooter data, and, upon close inspection, are marginally visible in the noisy red ISIS spectrum. Both red spectra are shown in Figure 5, along with SDSS 1228, the prototypical white dwarf with emitting metal gas and dust (Brinkworth et al. 2009; Gänsicke et al. 2006). Notably, the Ca II line profiles for this star are substantially narrower and weaker compared to those detected in the other three published cases. In 0959 the full width at

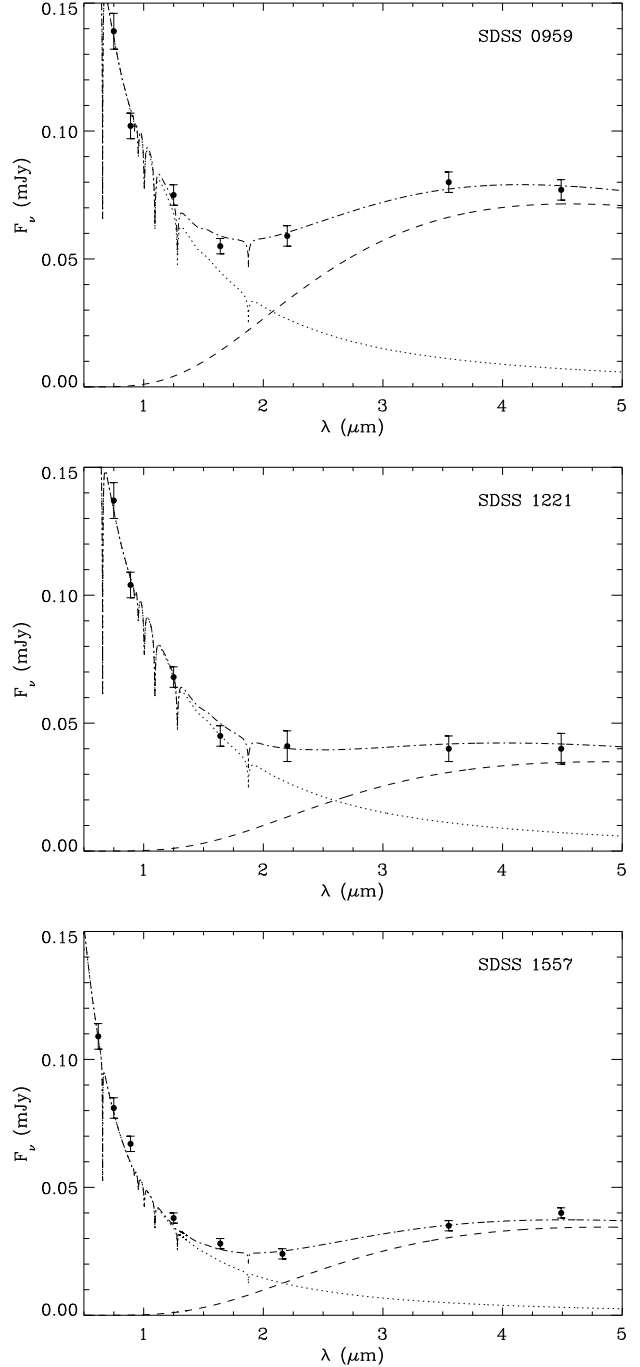


Figure 4. Infrared excesses fit by circumstellar dust disk models whose parameters are listed in Table 4. The plot features are the same as in Figure 2, but on a linear scale to emphasize the infrared excesses. Dashed lines represent emission from optically thick, flat disk models, and the dashed-dotted lines represent the sum of the stellar and circumstellar model fluxes.

zero intensity and equivalent width are close to 250 km s^{-1} and 3 \AA , respectively, while the known cases have values in the range $1000 - 1400 \text{ km s}^{-1}$ and $10 - 60 \text{ \AA}$ (Melis et al. 2010; Gänsicke et al. 2008, 2007, 2006). Assuming that the structure of the gas disks in 0959 and 1228 are similar, the velocity width of the Ca II lines in the two systems can be

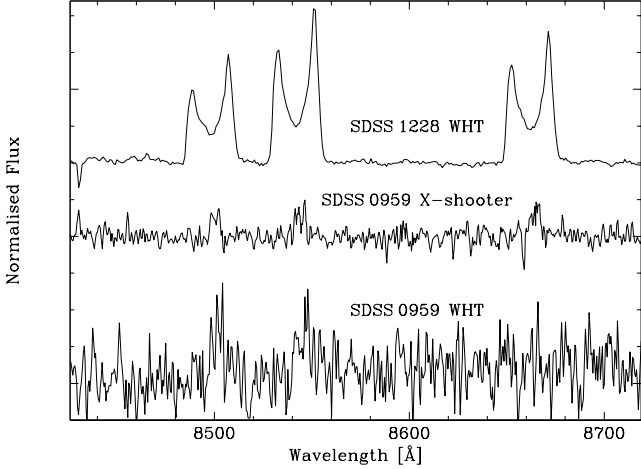


Figure 5. The Ca II triplet region of 0959 in the normalized WHT and X-Shooter spectra exhibit clear emission lines from a gaseous disk component. For comparison, also plotted is the normalized spectrum of the prototype gas disk around SDSS 1228 (Gänsicke et al. 2006). The narrower emission features at 0959 indicate a disk that is significantly inclined relative to that seen at 1228, and consistent with the high fractional infrared luminosity measured with IRAC.

used to estimate the inclination of the disk orbiting 0959. For 1228, two independent estimates yield an inclination of 70° (Melis et al. 2010; Brinkworth et al. 2009), and this yields $i \approx 12^\circ$ for 0959. The independently estimated disk inclination from the model fitted to the infrared emission is 10° , consistent with a near face-on disk of dust and gas. Gänsicke et al. (2006) found that the Ca II emission lines in 1228 are optically thick, and hence a low disk inclination will naturally result also in a lower equivalent width.

SDSS 0959 becomes the fourth published case of a white dwarf with detectable, gaseous debris in addition to solid dust particles in a circumstellar disk (Melis et al. 2010; Farihi et al. 2010b; Brinkworth et al. 2009). At $T_{\text{eff}} = 13\,300\text{ K}$ it is by far the coolest star to host such dual-phase debris, demonstrating conclusively that the *detected* gas in dust disks is *not* related to grain sublimation in the presence of higher temperature white dwarfs. In the three well-studied cases, the gaseous and solid debris are essentially spatially coincident (Melis et al. 2010; Brinkworth et al. 2009), both spanning a region from around 20 to 100 stellar radii (Gänsicke et al. 2006). Critically, there is a distinct lack of emission from gas in the innermost regions where sublimation is expected, and which may be due to lower disk surface density, resulting from enhanced viscosity and inward drift of gas (Melis et al. 2010). Corroborating this picture, sublimation of dust at 0959 is expected only within 15 stellar radii, and hence cannot account for emitting gas out to 100 radii.

It is uncertain if the current disk at 0959 and other gas-dust disk hosts are recently created or extant disks that have been impacted by a additional body or material. Regardless, the presence of detectable gas is almost certainly related to the destruction of solid material.

3.1.2 1221

The IRAC images of this star reveal a point-like source neighboring the white dwarf. Both sources were simultaneously modeled and deconvolved with PSF-fitting photometry. The neighbor is faintly but clearly visible in the UKIDSS *H*-band image, and is identified as a separate source in that survey. The LIRIS *K_s*-band images place it $1''.8$ distant at position angle 256° . Together with its IRAC fluxes, the *JHK* photometry of the neighbor yields colors inconsistent with a (substellar) companion (Patten et al. 2006). Although relatively faint, it appears to be diffuse and extended in the ground-based images and is thus a background galaxy. Both the UKIDSS and LIRIS photometry of the white dwarf reveal strong infrared excess at *K*, with the latter dataset confidently free of photometric contamination by the neighbor, in agreement with the excess determined from IRAC photometry. No Ca II lines are detected in the low S/N red ISIS spectrum.

3.1.3 1557

The mass of the white dwarf in 1557 is significantly below the average mass of field white dwarfs (Liebert et al. 2005). While the fit to the SDSS spectrum is consistent with a low-mass, carbon-oxygen core, the WHT data are more suggestive of a helium core. The SDSS data are of relatively poor quality at $S/N \approx 10$, while the WHT spectrum has $S/N \approx 30$. Table 1 lists the weighted average of these two solutions, favoring the low mass interpretation. If a low surface gravity is corroborated in future observations, this may signify an innermost planet that was consumed during the first ascent giant phase, ejecting sufficient envelope mass to prevent the onset of helium ignition (Nelemans & Tauris 1998). This picture is consistent with the evidence presented here for a remnant planetary system. As in the case of 1221, no Ca II emission is seen in the poor quality ISIS data.

3.2 Unusual Near-Infrared Colors for 1159

This DQ peculiar star (LP 494-12, WD 1156+132) was selected on the basis of independent *JHK* photometry that revealed a 0.3 mag excess at *K* band (Farihi 2009) relative to model expectations for a 10 000 K, helium atmosphere white dwarf (Holberg & Bergeron 2006; Fontaine et al. 2001); its UKIDSS photometry independently corroborates this result. Due to the C_2 absorption features at blue-green wavelengths, a pure helium atmospheric model was fitted only to the *izJH* photometric data, as shown in Figure 6. The IRAC fluxes reveal only a Rayleigh-Jeans tail to the spectral energy distribution, but at a shifted, lower temperature relative to the $0.6 - 1.5\,\mu\text{m}$ continuum. As found for another DQp star (LHS 2293; Farihi 2009), this apparent excess is likely a re-distribution of emergent flux due to the highly absorbed regions within the atmospheric C_2 bands. Thus the infrared excess only exists relative to a pure helium atmosphere, and is likely due to a distinct, absorption-induced shape in the energy distribution of the star.

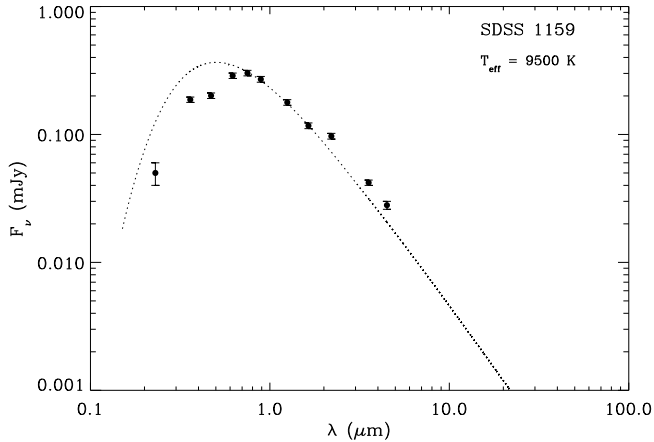


Figure 6. Spectral energy distribution of the DQ peculiar star LP 494-12, which has $H - K > 0.25$ mag in both UKIDSS and independently obtained photometry. Fitted to the $izJH$ photometry is a 9500 K stellar model for a pure helium atmosphere white dwarf (see §3.2).

3.3 A Likely Ultracool Companion at 1247

The infrared excess observed at this star is distinct, as the $3.6\,\mu\text{m}$ flux excess is strong, but the $4.5\,\mu\text{m}$ flux is consistent with a Rayleigh-Jeans type slope (see Figure 2). At first glance this may seem puzzling, but most M dwarfs approach this spectral behavior at IRAC wavelengths (Patten et al. 2006; Cushing et al. 2005). Neither the UKIDSS nor the IRAC images indicate an additional source (i.e., a spatially detectable companion), implying any secondary would have a projected separation smaller than around 70 AU, and essentially ruling out a background object as the cause of the observed emission. While the infrared excess is solid, and possibly apparent at J band, the S/N of the UKIDSS photometry is below 10 at H and K , making it hard to estimate a companion spectral type based on these data. Assuming the observed excess emanates from a companion at the correct distance, its 2.2, 3.6, and $4.5\,\mu\text{m}$ absolute brightnesses are 11.2, 10.0, and 9.8 mag. Comparing these values to the empirical absolute magnitudes of ultracool dwarfs at these wavelengths yields an approximate spectral type of $L0 \pm 1$ (Leggett et al. 2010; Patten et al. 2006; Vrba et al. 2004; Dahn et al. 2002; Kirkpatrick & McCarthy 1994) for a low mass companion. Superior JHK photometry would tighten up this estimate, and possibly indicate a new L-type companion to a white dwarf, which are rare (Steele et al. 2011; Farihi et al. 2005). Radial velocity monitoring of the white dwarf has the potential to detect variability if the system is a close binary, whereas high angular resolution imaging may be required if the system has a moderately wide separation.

3.4 A Likely Background Galaxy at 1320

The IRAC images of this star have full widths at half maximum that are inconsistent with a single point source; they are enlarged by about 20% in both channels and there is modest elongation in the $3.6\,\mu\text{m}$ image roughly along P.A. 45° . Nothing is seen in the UKIDSS images, but a second

source appears faintly in the LIRIS H and K_s -band images at a position consistent with the IRAC data. The image of this additional source is diffuse and extended and almost certainly a background galaxy. Moreover, there is an offset between the image centroids of the science target in the LIRIS and IRAC images, indicating that the IRAC source (and hence flux) is coincident with the additional source imaged with LIRIS, and not the white dwarf. The flux from this likely galaxy falls within $1''.0$ of the white dwarf, and contaminates all available infrared photometry. Even with PSF-fitting photometry on the LIRIS images, the resulting colors are slightly too red for a 20 200 K white dwarf. Given the overlapping proximity of this source to the white dwarf, the infrared excess is probably due entirely to this background object.

3.5 No Near-Infrared Excess for 1506

Somewhat ironically, the only star without a corroborated infrared excess via IRAC photometry is the brightest source in the sample, and thus the star with the *highest* S/N UKIDSS photometry. However, this star was selected for the *Spitzer* program when the evaluation criteria were still tied to UKIDSS DR4, and has since dropped out of the selection based on the release of DR8 and an improved analysis (Girven et al. 2011). The model for 1506 shown in Figure 2 shows that an excess is neither observed with *Spitzer*, nor in K -band. While this white dwarf was observed with ISIS, confirming its nature as a DA star, it is hence dropped from further analysis.

4 DISCUSSION AND CONCLUSIONS

4.1 An Unbiased Dust Disk Frequency

What makes this study so far unique is that previous IRAC programs have either targeted known metal-rich white dwarfs, or near-infrared bright white dwarfs. While the first approach has been highly successful and accounts for the bulk of white dwarf disk discoveries to date (Farihi et al. 2010b, 2009; Jura et al. 2007), two drawbacks exist. First, it requires 8 m class telescope time using high-resolution spectroscopy to efficiently identify (weak) metal lines in white dwarfs (Koester et al. 2005; Zuckerman et al. 2003), and second, only about 20% of metal-contaminated white dwarfs have disks (Farihi et al. 2009). The second method, employed by the Mullally et al. (2007) survey of more than 130 white dwarfs with $K_s < 15$ mag, was unbiased by the presence or absence of atmospheric metals, but only two stars with dust were found (von Hippel et al. 2007), and is hence only 1.5% efficient by number of targets. Here, five candidate DA white dwarfs with K -band excess have been selected with a success rate of 60% for circumstellar dust and 80% for confirmed infrared excesses physically associated with the system. One of five targets has an infrared excess probably due to a background galaxy.

Based on the candidate selection criteria and numbers given in Table 6 of Girven et al. (2011), of 1884 candidate and confirmed DA white dwarfs with the necessary UKIDSS detections, there are 12 stars whose data are consistent with disk-like, K -band excesses. Several years of *Spitzer* studies

have shown that only 50% of dusty white dwarfs have such *K*-band excesses (Farihi et al. 2010b), implying that a decent estimate of the disk fraction among DA white dwarfs is at least 1.2%. However, as seen in this study, in some cases the *K*-band data can be the result of neighboring background objects, as well as real companions such as low mass stars or brown dwarfs. Thus a more realistic estimate is 3/5 of this number, implying at least 0.8% of DA (and presumably all) white dwarfs have dust disks (and atmospheric metals), consistent with previous estimates (Farihi et al. 2009). These results only apply to stars with cooling ages less than 1 Gyr, as this corresponds to the approximate cutoff in effective temperature (8000 K; Fontaine et al. 2001) for the DA color selection. However, *Spitzer* studies have shown a distinct lack of dust disks at older and cooler metal-contaminated stars; only G166-58 has an (anomalous) infrared excess and a cooling age beyond 1 Gyr (Farihi et al. 2008b).

4.2 A Lack of *K*-Band Emitting Dust Disks at Warm to Hot White Dwarfs

Interestingly, the DA selection criteria is quite sensitive to warm to hot, hydrogen-rich white dwarfs, as the Balmer decrement gives these stars unique colors in that wavelength region (Girven et al. 2011). However, there are no candidates for dust among thousands of stars(!). Either dust disks at white dwarfs with $T_{\text{eff}} > 25000$ K exist yet rarely exhibit *K*-band excess or dust at such stars is itself rare. The latter possibility is somewhat contradictory based on the paradigm of planetary systems that are dynamically rejuvenated at the onset of the post-main sequence (Bonsor et al. 2011; Bonsor & Wyatt 2010; Debes & Sigurdsson 2002). If this apparent dearth of warmer systems at *K*-band is real, it would likely require a physical mechanism to preclude such emission (such as rapid removal of warm grains, or long timescales for dust disk spreading toward the star).

Farihi (2011) plot the fractional infrared luminosity of all known white dwarfs with dust circa mid-2010 as a function of cooling age, revealing a potential trend of increasing dust emission towards cooler stars. This could be a natural consequence of the potential for cooler white dwarfs to host wider disks: as a star cools and its luminosity decreases, dust grains may persist closer to the stellar surface prior to sublimation. Thus, any disk extending inward from the Roche limit has the potential to be wider at cooler white dwarfs. Conversely, at increasingly warmer stars, the inner dust disk edge will be physically further from the star as the radius at which grains are rapidly sublimated increases (see Table 4), eventually exceeding the Roche limit for large solid bodies (von Hippel et al. 2007). While it is uncertain at which precise effective temperature an evolving dust disk might be completely sublimated, the results of this work clearly show that disk emission analogous to G29-38 is rare among warm and hot white dwarfs. More sensitive surveys with *Spitzer* and *WISE* are needed to address this matter more comprehensively.

ACKNOWLEDGMENTS

The authors thank the referee Sandy Leggett for feedback which improved the quality and clarity of the manuscript. This work is based in part on observations made with the *Spitzer Space Telescope*, which is operated by the Jet Propulsion Laboratory, California Institute of Technology under a contract with NASA. Some data presented herein are part of the Sloan Digital Sky Survey, which is managed by the Astrophysical Research Consortium for the Participating Institutions (<http://www.sdss.org/>), and the UKIRT Infrared Deep Sky Survey.

REFERENCES

- Abazajian, K. N., et al. 2009, ApJS, 182, 543
- Bonsor, A., Wyatt, M. 2010, MNRAS, 409, 1631
- Bonsor, A., Mustill, A. J. Wyatt, M. 2011, MNRAS, 414, 930
- Brinkworth, C. S., Gänsicke, B. T., Marsh, T. R., Hoard, D. W., Tappert, C. 2009, ApJ, 696, 1402
- Cushing, M. C., Rayner, J. T., Vacca, W. D. 2005, ApJ, 623, 1115
- Davidsson, B. J. R. 1999, Icarus, 142, 525
- Dahn, C. C., et al. 2002, AJ, 124, 1170
- Debes J. H., Sigurdsson S. 2002, ApJ, 572, 556
- D’Odorico, S. et al. 2006, SPIE, 6269, 626933
- Eisenstein D. J., et al. 2006, AJ, 132, 676
- Farihi, J. 2009, MNRAS, 398, 2091
- Farihi, J. 2011, in White Dwarf Atmospheres and Circumstellar Environments, ed. D. W. Hoard (Berlin: Wiley-VCH)
- Farihi, J., Becklin, E. E., Zuckerman, B. 2005, ApJS, 161, 394
- Farihi, J., Becklin, E. E., Zuckerman, B. 2008a, ApJ, 681, 1470
- Farihi J., Barstow M. A., Redfield S., Dufour P., Hambly N. C. 2010a, MNRAS, 404, 2123
- Farihi, J., Jura, M., Lee, J. E., Zuckerman, B. 2010b, ApJ, 714, 1386
- Farihi, J., Jura, M., Zuckerman, B. 2009, ApJ, 694, 805
- Farihi, J., Zuckerman, B., Becklin, E. E. 2008b, ApJ, 674, 431
- Fazio, G. G., et al. 2004, ApJS, 154, 10
- Fontaine, G., Brassard, P., Bergeron, P. 2001, PASP, 113, 409
- Gänsicke, B. T., Koester, D., Marsh, T. R., Rebassa-Mansergas, A., Southworth J. 2008, MNRAS, 391, L103
- Gänsicke, B. T., Marsh, T. R., Southworth, J. 2007, MNRAS, 380, L35
- Gänsicke, B. T., Marsh, T. R., Southworth, J., Rebassa-Mansergas, A. 2006, Science, 314, 1908
- Girven, J., Gänsicke, B. T., Steeghs, D., Koester, D. 2011, MNRAS, 417, 1210
- Holberg, J. B., Bergeron, P. 2006, AJ, 132, 1221
- Hubeny, I., Lanz, T. 1995, ApJ, 439, 905
- Hunt, L. K., Mannucci, F., Testi, L., Migliorini, S., Stanga, R. M., Baffa, C., Lisi, F., Vanzì, L. 1998, AJ, 115, 2594
- Jura, M. 2003, ApJ, 584, L91
- Jura, M., Farihi, J., Zuckerman, B. 2007, ApJ, 663, 1285
- Jura, M., Farihi, J., Zuckerman, B. 2009, AJ, 137, 3191

- Kilic, M., von Hippel, T., Leggett, S. K., Winget, D. E. 2006, *ApJ*, 646, 474
- Kirkpatrick, J. D., McCarthy, D. W. 1994, *AJ*, 107, 333
- Koester D. 2010, In *Memorie della Societa Astronomica Italiana*, 81, 921
- Koester, D., Rollenhagen, K., Napiwotzki, R., Voss, B., Christlieb, N., Homeier, D., Reimers, D. 2005a, *A&A*, 432, 1025
- Lanz, T., Hubeny, I. 1995, *ApJ*, 439, 875
- Lawrence, A., et al. 2007, *MNRAS*, 379, 1599
- Leggett, S. K., et al. 2010, *ApJ*, 710, 1627
- Liebert J., Bergeron P., Holberg J. B. 2005, *ApJS*, 156, 47
- Manchado, A., et al. 1998, *SPIE*, 3354, 448
- Marsh, T. R. 1989, *PASP*, 101, 1032
- Martin, D. C., et al. 2005, *ApJ*, 619, L1
- McCook G. P., Sion E. M. 1999, *ApJS*, 121, 1
- Melis, C., Jura, M., Albert, L., Klein, B., Zuckerman, B. 2010, *ApJ*, 722, 1078
- Melis, C., Farihi, J., Dufuour, P., Zuckerman, B., Burgasser, A. J., Bergeron, P., Bochanski, J., Simcoe, R. 2011, *ApJ*, 732, 90
- Mullally, F., Kilic, M., Reach, W. T., Kuchner, M., von Hippel, T., Burrows, A., Winget, D. E. 2007, *ApJS*, 171, 206
- Nelemans, G., Tauris, T. M. 1998, *A&A*, 335, L85
- Patten, B. M., et al. 2006, *ApJ*, 651, 502
- Probst, R. 1981, Ph.D. Thesis, University of Virginia
- Probst, R. 1983, *ApJS*, 53, 335
- Probst, R. G., O'Connell, R. W. 1982, *ApJ*, 252, L69
- Rafikov, R. R. 2011, *MNRAS*, 416, L55
- Rebassa-Mansergas, A., Gänsicke, B. T., Rodríguez-Gil, P., Schreiber, M. R., Koester, D. 2007, *MNRAS*, 382, 1377
- Steele, P. R., Burleigh, M. R., Dobbie, P. D., Jameson, R. F., Barstow, M. A., Satterthwaite, R. P. 2011, *MNRAS*, 416, 2768
- Vennes, S., Kawka, A., Németh, P. 2011, *MNRAS*, 413, 2545
- von Hippel T., Kuchner M. J., Kilic M., Mullally F., Reach W. T. 2007, *ApJ*, 662, 544
- Vrba, F., et al. 2004, *AJ*, 127, 2948
- Wang, Z., Chakrabarty, D., Kaplan, D. L. 2006, *Nature*, 440, 772
- Werner, M. W., et al. 2004, *ApJS*, 154, 1
- Zuckerman, B., Becklin, E. E. 1992, *ApJ*, 386, 260
- Zuckerman, B., Koester, D., Reid, I. N., Hünsch, M. 2003, *ApJ*, 596, 477